Evaluation of the ciprofloxacin adsorption capacity of common industrial minerals and application to tap water treatment

Mohamed Bizi, F.E. El Bachra

Evaluation of the ciprofloxacin adsorption capacity of common industrial minerals and application to tap water treatment

M. BIZI*, & F.E. EL BACHRA

BRGM Environment & Ecotechnologies Division

3, Avenue C. Guillemin, 45060 ORLEANS Cedex 2

* Corresponding author.

E-mail address: m.bizi@brgm.fr

Phone +33(0)2 38 64 36 62

Abstract

Many technologies exist to treat medication residues however their implementation in different types of treatment processes for wastewater and water intended for human consumption is balanced against their cost-effectiveness and faces technical difficulties. The contribution of a set of natural industrial minerals commonly used in filtration to the elimination of ciprofloxacin was evaluated. This amphoteric antibiotic is also widely found in hospital effluents. The best adsorption rates found in a non-competitive environment were obtained for MONADOR montmorillonite. This natural, inert, readily available mineral is known for its high crystallinity, its high cation exchange capacity (CEC) and its very high specific surface area. By taking into account the size and volume of the ciprofloxacin molecule, the principal component analysis clearly shows that the CEC is a determining factor in the elimination of this molecule and that the microporosity of activated carbon is not involved in this process. Adsorption in tap water, the innovative element of this study, shows that MONADOR <20 µm bentonite shows a mean CIP adsorption rate of 184 ±6 mg/g, and can therefore compete with activated carbon. This work constitutes the first stage in the qualification of low-cost industrial minerals for environmental protection in its broadest sense.

Keywords

Adsorption, ciprofloxacin, drinking water, isotherm, micropollutants, smectite.

1. Introduction

Today, environmental contamination by pharmaceutical micropollutants is a well-established fact. This contamination, which has been known for several decades [1,2], is currently a major concern across the globe. It represents a real scientific challenge in terms of ecotoxicity, public health, soil pollution, as well as drinking water and wastewater management strategies. The presence of pharmaceutical products in the environment can be caused by their manufacture, formulation, distribution, use or disposal. When medication is consumed, it is metabolised in proportions ranging from 10 to 90%. A non-negligible quantity of active ingredient is therefore excreted, mainly in urine, and enters wastewater in urban areas, or is directly released into the environment in the case of livestock farms. 70% of antibiotics ingested end up in the natural environment. Various studies have confirmed the presence of a large number of medicinal substances in all the environmental compartments: surface waters, soil, sediment and groundwater [1,2].

According to the type of medicinal substance and the different water categories, the concentrations found will vary within a bracket ranging from one nanogram per litre in fresh or marine surface waters, groundwater and water intended for human consumption, up to a microgram, or even several hundred micrograms per litre in effluents and residuary waters, with spatio-temporal variations depending on human activities. Several authors have found pharmaceutical molecules in drinking water [1]. A compilation of the concentrations of pharmaceutical pollutants found in the environment by country is presented in a database developed by the German Federal Environment Agency [3].
Furthermore, many categories of antibiotics and anticonvulsants are quite often present in surface waters, including carbamazepine, ciprofloxacin and sulfamethoxazole. As concerns hospital wastewater, the most concerning substances found are anti-cancer drugs, certain antibiotics and contrast agents. Hartmann [2] detected ciprofloxacin concentrations ranging from 3 to 87 µg/L in the wastewaters of certain hospitals. A recent study conducted over a 4-year period [4] has shown that the molecules found in significantly higher concentrations in hospital effluents than in urban effluents are: paracetamol, ketoprofen, non-ionic detergents and the three antibiotics ciprofloxacin,

sulfamethoxazole and vancomycin. The difference in concentrations is more marked for these three antibiotics, with concentrations at least 10 times higher in hospital effluents.

Ciprofloxacin (CIP), which belongs to the group of fluoroquinolones, is of particular interest because of its omnipresence in hospital effluents, in wastewaters and in surface waters at concentrations ranging from ng to mg/L. Near certain pharmaceutical factories, it can reach concentrations of up to 30 mg/L [6]. This antibiotic is also found in water intended for human consumption. Like most antibiotics, CIP has been shown to be relatively resistant to biodegradation and genotoxic for aquatic organisms [7]. Their presence in water, even at low concentrations, can promote the appearance of resistance in pathogenic bacteria [8] and can trigger inhibition in activated sludge plants. Conventional water treatment processes are relatively ineffective at totally eliminating antibiotics and present-day wastewater treatment plants are not designed for this application. Furthermore, ozone or chlorine treatment can lead to the production of degradation by-products or metabolites which must be taken into consideration to assess their potential biological effects. Membrane filtration processes such as nanofiltration or reverse osmosis, suited to certain sizes and molecules, remain very costly processes and require partial remineralisation of the water.

In a bid to provide a solution to this issue, studies have been conducted to determine the potential of a set of natural or synthetic minerals to eliminate ciprofloxacin by adsorption. The main materials investigated are Aluminium, iron hydrous oxides and Goethite [9], Carbon nanotubes [10], Illite, Rectorite and Montmorillonite [11], Kaolinite [12], Coal fly ash [13], Activated carbon, carbon xerogel and carbon nanotubes [14], graphene oxide/calcium alginate [15], Magnetite [16], and Birnessite [17]. Of all these products, only montmorillonite and activated carbon have shown high adsorption rates, of interest for water treatment processes. The other products showed low, very low or even insignificant adsorption rates for this application. Furthermore, the use of nanoparticles (size <100 nm) in this context is strongly advised against. They belong to a group of so-called "emerging" substances which are currently raising questions as to their environmental and health impact. Titanium oxide, whether nanometric or micrometric, is also concerned. It is classified as a possible carcinogen for humans and animals.

All of the different above-mentioned adsorption studies were conducted in the laboratory in closed environments (bottle or flask) with Milli-Q water and montmorillonites of less than 2 µm extracted from raw clay pre-screened at 80 µm, by centrifugation or sedimentation according to Stokes's law. Industrially, this grain-size fraction is excessively costly to produce. Technically, there are two industrial methods of producing a grain-size fraction, with a high montmorillonite concentration, close to this dimension: (i) dry classification using an Alpine ATP50 air flow classifier (<2 to 5 µm) or (ii) separation by hydrocycloning (< 5 to 8 µm). This grain-size fraction only represents 10 to 30% by mass of the clay fraction <80 µm at the most. The overall cost of its preparation would therefore be similar to that of activated carbon ($300-1000/ton), which itself is non-negligible for water treatment. In light of this information and with respect to economic constraints, we chose to examine the contribution of a clay fraction of less than 20 µm (<20 µm), extracted by sieving smectite-rich clay, to the elimination of CIP. The aim was to select the most suitable clay based on its CIP adsorption performance, from among three industrial smectites: MONADOR, Rassoul and SWy3. Their retention classification was also compared to that of a diatomite, a kaolin, two powdered activated carbons and the two <20 µm fractions of these activated carbons. These industrial products were chosen in order to: (1) select the best smectite and classify it in relation to the most commonly used industrial adsorbents, (2) determine the adsorption capacity of the chosen products in an open environment (jar test) with strong agitation (G=600 s^{-1}), similarly to industrial practices, (3) determine the impact of the CEC and solid porosity on CIP's adsorption performances, and (4) generate adsorption isotherms both for pure water (Milli-Q) and tap water. It is worth highlighting that the literature does not currently offer any data on CIP treatment in tap water. It should also be recalled that water treatment is generally implemented at between pH 6.5 and 9.

2. Materials and methods

The industrial products chosen to achieve the above-stated objective were:

- **Two powdered activated carbons**, AquaSorb XP17 (CAP1), marketed by JACOBI CARBON COMPANY Sweden and NORIT SA SUPER (CAP2), marked by Cabot Corporation USA (CAP1). Both have been developed to treat water intended for human consumption and are generally introduced continuously into water at a concentration of 10 to 25 mg/L. CAP1 is obtained from coconut and CAP2 from peat. They have a particle size of less than 120 µm and an average diameter of around 24 µm. 50% by mass of CAP1 is less than 20 µm compared to 56% for CAP2.

- **One diatomite** from the region of Awinate in the centre of Morocco in the Middle Atlas. This is porous, low density sedimentary rock almost entirely formed from the microscopic skeletal remains of diatoms. The major component of this material is amorphous silica.

- **Kaolin K7A,** from the Ploemeur deposit in the Morbihan, France, and generally used in paper coating. This kaolin is composed of around 91% kaolinite and 9% mineral impurities (Illite, Muscovite and Quartz). 80% by mass of this kaolin has a particle size of less than 2 µm. The fact that kaolinite is a dioctahedral clay with a T/O structure (stacking of a tetrahedral layer and an octahedral layer) prevents all swelling caused by intercalation in the interlayer space. However it is exactly this type of parameter that will be used to distinguish between the adsorption capacities of the selected smectites.

- **Two bentonites** rich in montmorillonite (dioctahedral smectite). The first, MONADOR, came from a deposit in the north of Morocco in the province of Nador, while the second, SWy3, came from Crook County Wyoming and was supplied by the Source Clays Repository of the US Clay Minerals Society.

- **Rassoul clay,** very high in stevensite (trioctahedral smectite), which came from the world's only deposit located in Morocco, south-east of the Missour tertiary basin.

In their raw state, the latter three clays contain mineral impurities in increasing concentrations from the fine grain fraction to the coarse fraction. The two bentonites contain quartz and feldspar, among others, and Rassoul contains quartz and dolomite. These impurities, even in low proportions, can be limiting factors for adsorption and swelling processes in the mineral, thus reducing the cation exchange capacity.

The two montmorillonites and the stevensite concentrated in the colloidal fractions <2 µm of these clays were extracted by wet elutriation. The separation of the Rassoul clay was preceded by complete cation exchange with NaCl to promote electrostatic repulsion between particles and to increase the dispersion of the Rassoul suspension. This procedure (sodium homoionization) was essential for performing the elutriation of this product. In terms of the sedimentation and centrifugation, the elutriation resulted in large quantities of smectites of better mineralogical quality (relatively few mineral impurities) being obtained. The fractions obtained were MONADOR-2, SWy3-2 and Na-Rassoul-2. For practical reasons outlined below, only MONADOR-2 was subsequently homoionized with sodium and calcium to give Ca-MONADOR-2 and Na-MONADOR-2. The fractions with a particle size of less than 20 µm were prepared by sieving. The purpose of this selection and preparation process was to cover as wide a range as possible of CECs and porosities.

The cation exchange capacity (CEC) of each clay in this study was determined according to the AFNOR NF X 31-130 [18] standard using hexaamminecobalt(III) chloride $Co(NH_3)_6Cl_3$ as the salt whose hexaamminecobalt cation can displace the cations naturally fixed by the sample. The hexaamminecobalt ion has a very high capacity to displace all exchangeable cations. The concentration of free hexaamminecobalt ions remaining after exchange and filtration was determined in the filtrate by colorimetry at 475 nm. The CEC is expressed in milliequivalents per 100 grams of clay calcined at 1000 °C. This is an intrinsic characteristic of each clay. In the case of smectites, it is

related both to the permanent charge and the pH-dependent charge. It therefore represents the sum of the number of ions adsorbed between the sheets of the clay structure and those adsorbed on the external surfaces.

The PZC (point of zero charge) that is the pH at which the net charge density due to proton adsorption/desorption (σ_H) at mineral surface is equal to zero, was determined using the Mular-Roberts (MR) method [19], known as the pH drift method. The experiment was conducted at 25 ±1°C, in a glove box, protected from atmospheric CO_2. Inside the box, nine 50 ml bottles, individually filled with 20 ml of Milli-Q water (18.2 MΩ/cm) free from CO_2, were adjusted to pH values ranging from 3 to 11 with a step of around one unit. HCl and NaOH were used for this purpose. At equilibrium, 0.1 g of dry solid was added to each bottle and all the bottles were agitated for 24 hours. At the end of this cycle and after settling, the pH of each suspension was carefully measured. On the graph illustrating ΔpH ($pH_{Final} - pH_{initial}$) as a function of the initial pH, the PZC corresponds to the value at which ΔpH is equal to the initial pH. This physico-chemical parameter provides essential information on the adsorption and stability characteristics of the adsorbates. In the case of kaolinite and smectites, the PZC exactly matches the point of zero net proton charge (PZNPC). Like the PZC, the PZNPC depends on the species specifically sorbed. The electrophoretic mobility was measured using the Malvern Zetasizer Nano ZS.

The specific surface areas and the pore volumes of the different products were determined at 77 K from N_2 gas adsorption/desorption isotherms with a discontinuous volumetry sorptometer, Micromeritics ASAP 2050. Prior to analysis, the samples were dried and degassed at 200°C until a residual vacuum of less than 0.02 mbar was obtained using the VacPrep 061 Micromeritics system. The BET method was used to determine the specific surface areas based on a value of 0.162 nm² for the molecular cross-sectional area of nitrogen at 77 K. The t-plot method was used to assess the microporosity of samples from the desorption isotherms.

The chemical composition presented in this article was determined by the combination of X-ray fluorescence for the major elements, atomic absorption for MgO and chemical volumetric analysis for ferrous iron.

The mineralogical compositions were determined by X-ray diffraction (XRD) from disoriented powders using the BRUKER D8 Advance Da Vinci diffractometer equipped with a copper radiation anticathode CuKα1 (λ=1.5418 Å). Diffractograms were obtained in the 2θ angular range between 2 and 76° with a sweep rate of 0.02° 2θ/s and a counting time of 710 s per step. The samples examined had been previously dried and degassed at 200 °C. XRD was also used to characterise ciprofloxacin adsorption by the clay based on the evolution of the basal distance (001). Analysis was performed before and after CIP adsorption between 2 and 15° 2θ, on oriented layers produced with thoroughly washed samples dried at 60 °C. All the diffractograms were smoothed at less than 3% using the Savitsky and Golay method, a baseline subtraction, then standardisation in relation to the total area.

Finely dispersed powder of ciprofloxacin ($C_{17}H_{18}FN_3O_3$) with high purity (>99.9%) was purchased from Sigma Chemical (Product Number 17850, CAS number 85721-33-1) and was used as received. Its molecular weight and melting-point temperature are 331.34 g mol^{-1} and 268 °C respectively.
Ciprofloxacin ″CIP″, a fluoroquinolone antibacterial agent, contains a secondary alkylamine, two tertiary arylamines (aniline-like amines), and a carboxylic acid. It has one fluorine, which is conjugated to the carboxylic acid functional group (Fig.1) [20]. With these multiple functional groups, CIP possess both acidic and basic character. It is a zwitterionic compound with acid dissociation constants of 6.0 ±0.1 (pka_1) and 8.8 ±0.1 (pka_2). As shown in Fig. 2, CIP is primarily cationic below pKa1, anionic above pKa2, and zwitterionic (net neural) between pka_1 and pka_2. Percent ionization (PI) is giving by Henderson-Hassalba Equation

$$PI = \frac{100}{1+10^{x(pH-pKa)}} \qquad (1)$$

Where x = -1 and pka = pka_1 if acid drug or x = 1 and pka = pka_2 if basic drug

The aqueous solubility of CIP is pH-dependent, due to the presence of the carboxylic and NH groups of piperazine, with the zwiterionic and unionized forms being dominant at neutral pH. It is well-known that the solubility of a zwitterionic compound depends on its ionization constants and intrinsic solubility.

According to Ray Davidson & al. [21], and for a solvent whose concentration is much higher than that of the solute, the solubility of a zwitterionic compound with two ionizable groups can be expressed by

$$S_T = S_0\left(1 + 10^{(pKa_1 - pH)} + 10^{(pH - pKa_2)}\right) \qquad (2)$$

Where S_T is the total solubility, S_0 is intrinsic solubility; K_{a1} and K_{a2} represent the thermodynamic macroscopic dissociation constants.

The intrinsic solubility of ciprofloxacin, that is, the solubility of the neutral form, depends on the temperature [21]. Between 6 and 40 ° C, S0 can be determined from the following equation:

$$S_0^{0.5} = a + bT^{1.5} \qquad (3)$$

Where a= 0.178113, b= 0.0009253, T in ° C and S_0 in mg/ml

As an adsorbate, CIP was measured by UV-Visible spectrometry. The absorption spectrum of this molecule is characterised by several absorption bands all located in the UV band with varying intensities and positions according to the pH (Fig. 3). The optical density of the most intense absorption band due to electronic transition $\pi \rightarrow \pi^*$ was used, via a calibration curve, to deduce the quantities of CIP adsorbed by the powders based on the remainder method. For each physico-chemical

condition (pH and type of water) and in accordance with the Beer–Lambert law, a calibration curve was produced with 10 CIP concentrations between 0 and 20 mg/L. The coefficient of correlation, R^2, of each linear regression greatly exceeds the value 0.999.

The best CIP adsorbent was selected from among the 14 products proposed using a jar test of six stations fitted with single-blade stirring paddles in the form of square stainless steel sheets and open reactors with four baffles, geometrically similar, with a working volume of 809 mL. Two series of adsorption tests were run, one at pH 3 ±0.1 and the other at pH 6.5 ±0.2. The reactors filled with the suspension prepared with Milli-Q water containing 50 mg/L of mineral and 20 mg/L of CIP were agitated for 48 hours at an average speed gradient of 600 s^{-1} and at a temperature of 19 ±1°C. Following this step, a 40 ml sample from each reactor was centrifuged at 20,379 g for 30 min, filtered with a 0.1 µm PVDF syringe filter, then measured by UV spectrometry.

The trials intended to establish equilibrium adsorption isotherms were carried out in closed bottles with an internal diameter of 7 cm and a 600 ml capacity, filled with 550 ml of the suspensions to be filtered. For each experimental configuration defined by its pH and its water type, the bottles were filled with a suspension prepared with 50 mg/L of adsorbent and increasing CIP concentrations. All the bottles then underwent vertical agitation at 400 rpm using cylindrical magnetic PTFE bars (8x40 mm) for 48 hours at room temperature (20 ±1°C). At the end of this process, a sample from each bottle was centrifuged, filtered, then quantified by UV spectrometry. The adsorption isotherm was obtained by the graphic representation of the quantity of CIP adsorbed by the mineral "Qe" according to the residual CIP concentration in the equilibrium solution "Ce" [Qe=f(Ce)].

Given the texture and the energetic heterogeneity of the adsorbent surface, the adsorption isotherm models of Sips and Dubinin-Astakhov (D-A) were used to describe the adsorption equilibrium characteristics.

Sips and Dubinin-Astakhov (D-A) adsorption isotherm models were used to describe the equilibrium characteristics of adsorption. The Sips model [22] is a combination of the Langmuir and Freundlich isotherm models as shown in Equation 10.

$$Q_e = Q_{\max} \frac{(K_s C_e)^{n_s}}{1 + (K_s C_e)^{n_s}} \qquad (4)$$

Where, Qe is the amount of pollutant adsorbed per gram of the adsorbent at equilibrium (mg/g), Qmax is the maximum monolayer saturation capacity (mg/g), Ce is the equilibrium concentration of adsorbate (mg/L), K_s is the affinity constant (L/mg), and n_s is the surface heterogeneity index (–), which varies from 0 to 1. When n_s equal unity, the Sips isotherm returns to the Langmuir isotherm and predicts homogeneous adsorption. On the other hand, deviation of n_s value from the unity indicates heterogeneous surface. Also, when the denominator equals unity, the model resembles the Freundlich model.

The Dubinin-Astakhov model does not assume that the surface is homogeneous or that the adsorption potential is constant, as is the case for the Langmuir model. Its theory of volume filling of micropores is based on the fact that the adsorption potential is variable and the free enthalpy of adsorption is related to the degree of pore-filling. This isotherm assumes that the surface is heterogeneous and is expressed as follows:

$$Q_e = Q_{\max} \exp\left[-\left(\frac{\varepsilon}{E\sqrt{2}} \right)^n \right] \qquad (5)$$

$$\varepsilon = RT \ln\left(1 + \frac{1}{C_e} \right) = \Delta G \qquad (6)$$

Q_e is the amount of pollutant adsorbed per gram of the adsorbent at equilibrium (mg/g), Q_{max} is the maximum monolayer saturation capacity (mg/g), C_e is the equilibrium concentration of adsorbate (g/g), ε is the Polanyi potential (kJ/mol), E is the mean free energy of sorption (kJ/mol), n is the surface heterogeneity index, R is the universal gas constant (8.314 J/ mol °K), and T is the absolute temperature (°K).

D-A parameters were determined by transforming the D-A equation (5) into linear form:

$$\ln(Q_e) = \ln(Q_{\max}) - \left(\frac{RT}{E\sqrt{2}}\right)^n \left[\ln\left(1+\frac{1}{C_e}\right)\right]^n \qquad (7)$$

The slope of the plot of ln(Qe) versus $(\ln(1+1/Ce))^n$ gives the mean adsorption energy E, and the intercept yields the adsorption capacity Q_{max} (mg/g).

$$E = \frac{RT}{\sqrt{2}} \frac{1}{(slope)^{1/n}} \qquad (8)$$

The adsorption energy E was used for estimating the type of adsorption mechanism. For a magnitude of E between 8 and 16 kJ/mol, the adsorption process followed the chemical ion exchange, and values of E below 8 kJ/mol were charcteristic of a physical adsorption process [23].

3. Results and discussion

3.1 Characterization

It is well established that the efficacy of adsorbents in eliminating pollutants is dependent on their physical characteristics (particle size, porosity, and specific surface area), their surface chemistry and

the physico-chemistry of the carrier medium. The surfaces of the chosen adsorbents also comprise reactive amphoteric functional groups which can protonate or deprotonate depending on the pH value, meaning that they can have a different surface charge according to the pH of the solution in which they are present. Protonation and deprotonation reactions can be represented by the following equilibria:

$$S-OH + H_3O^+ \Leftrightarrow S-OH_2^+ + H_2O \qquad (9)$$

$$S-OH + OH^- \Leftrightarrow S-O^- + H_2O \qquad (10)$$

The term ≡SOH groups is used as a non-specific notation of amphoteric surface OH groups which carry a pH-dependent charge referred to as net proton surface charge.

As indicated in Fig. 1, CIP contains several functional groups with acido-basic properties and is therefore also amphoteric. The cationic form CIP^+ due to protonation of the amine group in the piperazine fragment is predominant when the pH of the solution is less than 6.0. When the pH of the solution is greater than 8.8, the anionic form CIP^- due to the loss of a proton from the carboxyl group is prevalent. When the pH of the solution is between 6.0 and 8.8, the zwitterionic form $CIP^{\pm}$ is the dominant species. The neutral form centred at pH 7.4, the point of zero charge for CIP, represents only 1% (Value determined from the ratio of surfaces, Fig. 2).

For a given texture, surface chemistry and ionic force, the pH will therefore directly control the CIP adsorption mechanisms. The properties and adsorption rate of this molecule will be dependent on the position of the pH in the suspension in relation to the point of zero charge, pH_{PZC}, of each component.

Within this context, the main parameters liable to be involved in ciprofloxacin adsorption mechanisms by the materials in this study are indicated in Table 1. The extent of each parameter is relatively broad. The CEC was found to be between 0.04 and 1.4, the PZC ranged from 4 to 9.2, the pore volumes were between 0 and 0.4 cm^3/g. The energy constant related to the normal adsorption energy of nitrogen varied between 300 and 1060. The high values obtained for the activated carbons show that they have

a high affinity for nitrogen and indicate the presence of a high microporosity. With the exception of this remark, this parameter should be used very cautiously given that it is the result of a very strong hypothesis that the probed surface is homogeneous. The BET specific surface area, referred to as the total surface area, is the sum of the external surface area and the surface area of pores accessible to nitrogen molecules. In the case of phyllosilicates, this surface area mainly represents the external surface.

However, the texture of the **activated carbons** is well described by the "nitrogen" probe. The specific surface areas of the micropores constitute the majority of the total surface areas of these carbons. The specific surface areas of the micropores make up (90%, 88%) in the case of (CAP1, CAP1-20) and (73%, 70%) for (CAP2, CAP2-20) of the total specific surface areas. This drop in microporosity between CAP1 and CAP2 coincides with an increase in CIP adsorption. Inversely, adsorption shows a linear increase as mesoporosity rises (R^2=0.99 for 4 points). This observation infers that adsorption on these carbons mainly occurs in the mesopores. CIP, qualified as a large molecule with a volume of 757.5 $Å^3$ [81], is mainly adsorbed in the mesopores and macropores.

At pH 3, the ciprofloxacin and the activated carbons were fully positively charged. The cationic form CIP^+ is due to protonation of the amine group in the piperazine fragment (Fig. 2). The positive charge of the activated carbons (Fig. 4) is mainly due to i) the initially alkaline oxygen or nitrogen functions and ii) the formation of electron donor-acceptor complexes of graphite planes which act as Lewis bases [24]. At pH 3, van der Waals interactions between these two products are predominant [83] and, in view of the polarity of CIP, it is not impossible that hydrogen bonds may occur.

At pH 6.6 ±0.1 adsorption by the carbons is increased. This increase may be due to the decrease in acidic oxygen functions at the activated carbons surface (Fig. 4) and probably to the decrease in water initially adsorbed at the surface, which prevented CIP diffusion in certain pores at acidic pH values. At pH 6.6, CIP had a 20% positive charge and an 80% neutral charge (Fig. 2), the zwitterionic form was therefore the dominant species. Hydrophobic interaction is the dominant adsorption mechanism at this

pH. In relatively low proportions, CAP2 and CAP2-20, which have a pH_{PZC} of 8.3, can promote van der Waals adsorption and hydrogen bonding. Given the configuration of the carbon surface at the point of zero charge, π-π electron donor-acceptor adsorption is entirely possible [26].

Awinate diatomite is composed of around 88.3% SiO_2, 3.7% Al2O3, 1.3% Fe_2O_3, 1.6 % (CaO, MgO, K_2O and SO_3) and 5% H_2O. Its surface is covered with a large number of Si−OH functional hydroxyl groups as well as a few Al−OH and Fe−OH hydroxyls. The amphoteric dissociation of these surface groups is responsible for the surface's electric charge. In very favourable physico-chemical conditions, the quantity of CIP able to be adsorbed in a single layer on a surface area of 9.85 m²/g is 6.77 mg/g, based on a molecular surface area of 80 Å² for CIP [28]. The quantities observed for diatomite therefore indicate a multi-layer condensation. The first layer is mainly adsorbed by hydrogen bonds, while the following layers are adsorbed by electrostatic bonds (+/-) between CIP molecules.

Kaolinite is a non-swelling, dioctahedral, 1:1 lamellar clay composed by the stacking of the elementary sheet formed by a tetrahedral layer (SiO_4) and an octahedral layer (AlO_6). Its lateral faces mainly comprise silanol groups ≡SiOH and aluminol groups =AlOH, responsible for the majority of its exchange capacity and its stability in suspension. These amphoteric edge sites show non-negligible retention properties for certain ions. The electrokinetic properties of the lateral faces may, as an initial approximation, be represented by a combination of the electrokinetic properties of quartz and α-alumina. The basal faces, composed either of oxygen ions organised into a hexagonal network or of a compact assembly of OH^- ions [29], can harbour a permanent electric charge in the case of isomorphic substitution in the network. The departure from electrical neutrality is offset by interlayer cations such as sodium and calcium. However, the work of Siretanu et al [30] on kaolinite KGa-1 using high resolution atomic force microscopy showed that pH also affects part of the basal faces. The electric charge of the tetrahedral basal face can vary from -0.016 to -0.044 e/nm² in the pH range from 4 to 9; and that of the octahedral basal face can range from +0.018 to +0.004 e/nm² for a pH ranging from 4 to 6 and have a value of -0.028 e/nm² at pH 9.

In view of their particle shape and size and their crystallography, kaolinites, like montmorillonites, develop surface energy heterogeneity. The use of the Langmuir isotherm by many authors to characterise the adsorption mechanisms of certain pollutants by phyllosilicates is therefore not always appropriate. This character can be illustrated by a revision of the isotherm of ciprofloxacin adsorption by kaolin KGa-2 produced by Li et al [12] at pH 3.5. Using the Langmuir equation, these authors determined that adsorption occurred in a single homogeneous layer with a maximum CIP adsorption capacity of 19 mmol/kg. As indicated in Fig. 5, the adjustment of experimental data with the Langmuir equation is not appropriate and, what's more, it underestimates the maximum adsorption value. The use of Sips and D-A equations proves to be better suited and more effective for this situation. The maximum adsorption capacity of kaolinite is 26.4 ±0.5 mmol/kg.

Furthermore, two phenomena can be easily distinguished in this Figure: (i) a vertical increase in the degree of coverage of negative basal faces for a residual concentration at zero equilibrium. The total adsorption achieved during this first phase was around 10 mmol/kg; (ii) a step, indicated by a change in slope occurring at around 4.5 10^{-3} mmol/L, marks the beginning of the second phase. This phase resulted in a total adsorption of 16.4 mmol/kg.

Based on the fact that the CEC of kaolinite is mainly due to its lateral faces and that the dimension of the projected surface area of CIP^+ is far higher than the interlayer space of kaolinite (0.3 nm [31]), CIP^+ cannot access this space and positions itself on this mineral in two stages. First, adsorption occurs by normal electrostatic interaction between CIP^+ and the negative basal surfaces, followed by adsorption on the rest of the surface by cation exchange [12]. At pH 3.5, the aluminol sites are fully positive and some of the silanol sites are negatively charged by SiO- [32]. The cation exchange and adsorption of CIP^+ therefore take place at SiO- sites. This analysis also applies to kaolin 7A at pH 3, whose CEC is 45 $mmol_C$/kg.

The point of zero charge (PZC) of kaolin 7A, i.e. its lateral faces, is equal to 4. Below pH 4, these faces are positive and above this value, they are predominantly negative and their rate increases as the pH rises (4 to 9). They are fully negative when the pH is greater than 9 (PZC of alumine). The maximum adsorption capacities of kaolin at pH 3 and pH 6.7 were found to be 145 and 133 ±2 mmol/kg respectively. At pH 3, adsorption occurred as previously by electrostatic interaction. The projected surface area involved in this mechanism was around 17 Å² [33]. At pH 6.7, the negative charge of lateral surfaces is due to the dissociation of MOH sites which behave as proton donors to result in MO^- sites. At this pH, 20% of CIP, in the form of CIP^+, is adsorbed by electrostatic interaction on the negative parts of the basal faces and on the MO^- sites of the lateral faces. The remaining 80%, which is neutral, is adsorbed through hydrogen bonds. The projected surface area of CIP at this pH was 80 Å² [28]. Kaolin 7A adsorbed more than kaolin KGa-2 given that it contains 5.3% illite (a highly reactive mineral) and also has a higher CEC.

Smectites (Table 1) generally feature three types of sites: cation exchange sites located on the basal surfaces, which have permanent negative charges due to isomorphic substitutions, then silanol ≡Si–OH sites and aluminol≡Al–OH sites, both located at the sheet edge and able to ionise according to the pH of the environment. The electric charge of these amphoteric sites becomes increasingly positive starting from the PZC of the lateral faces and moving towards pH 2, and increasingly negative starting from the PZC and moving towards pH 10. The PZC value of each smectite depends on its chemical composition and its crystallographic structure. Quantitatively, the most prevalent interaction process with ciprofloxacin continues to be cation exchange, but the amphoteric edge sites show non-negligible retention properties towards this molecule according to pH. While the specific surface areas of these smectites are high in relation to diatomite and kaolins, they only indicate the surface areas accessible to nitrogen and mainly represent the surface areas of mesopores and part of the surface areas of micropores. The inner surface concerned by CIP adsorption (cation exchange) cannot be determined using the BET method. The CIP adsorption rate increases with CEC and also depends on the nature of the exchangeable cations. The results show that the adsorption capacity of MONADOR montmorillonite is higher than that of all the other clays.

Furthermore, the monoionic sodium form of the clay MONADOR -2µm promotes the incorporation of a CIP rate greater than practically all of the products studied. It is worth noting that, due to its hydration capacities, the compensating cation controls the swelling and expansion of the clay's interlayer space [34,35]. On the other hand, the binding strength of the cations with the clay surface depends on the cation's hydration energy, ionic size, charge, and polarizability. According to Swartzen-Allen [36], the interaction strength of the main alkaline and alkaline earth ions with the clay surface increases in the following order: $Li^+ < Na^+ < K^+ < Rb^+ < Ca^{2+} < Cs^+$. Hydration enthalpies of Na^+ and Ca^{2+} are respectively -406 kJ. Mol^{-1} and -1579 kJ/mol [37]. The polarizabilities are 0.9947 for Na^+, and 3.161 for Ca^{2+} [38]. A high cationic charge, a high polarizability, or a high hydration energy are generally responsible of the strength of the bonding forces between a cation and a negatively charged surface. Na^+, less charged, of lower polarizability and of lower hydration enthalpy, will therefore tend to leave more easily the interlamellar space for a possible cationic exchange. Water molecules in the interlayers of Na-Montmorillonite had a larger self-diffusion coefficient than those of Ca-Montmorillonite at the same water content. Moreover, Na^+ had a higher self-diffusion coefficient than Ca^{2+} [39]. Compared to Ca^{2+}, Na^+ is liable to destabilise the sheet structure. This less charged cation therefore has a lower tendency to screen the interlayer permanent-charge of the smectite. Its presence causes high repulsive forces and causes the particles to repel each other. This leads to an increase in the negative charge in the suspension and facilitates cation exchange with CIP^+ through stronger electrostatic attraction. On the contrary, some calcium ions remain immobile, near the basal surfaces, and thereby reduce cation exchange. Replacing Na with Ca in MONADOR-2 also caused a decrease in micropore volumes and surface areas of the sample (Table 1). Consequently, Na-MONADOR-2 adsorbs more than Ca-MONADOR-2. MONADOR smectite was hence selected for this type of adsorption.

The mineralogical characterisation of the MONADOR -2µm fraction, which represents more than 85% by mass of the -20 µm fraction, was determined through a combination of chemical analyses of MONADOR-2, Na-MONADOR-2, Ca-MONADOR-2 dried at 200 °C and the X-ray diffraction of

MONADOR -2µm dried at 200 °C (Fig. 6). Based on monoclinic symmetry, this combination shows that MONADOR-2µm is composed of around 98% dioctahedral smectite (d_{060} = 1.50 Å), 1.8% albite and 0.2% quartz. Its interlayer (inter-reticular) distance d(001) is 9.98 Å, indicating predominantly dehydrated sheets (0-water layer). The full width at half-maximum intensity (FWHM) of the 001 reflection indicates that this smectite is less well crystallized than the smectite SWy-3. In a dehydrated state without any layer of water between the sheets (0W), the FWHM's are 1.368 for MONADOR-2 and 0.879 for SWy-3. Using XRD diffractogram, the (a, b, c) dimensions at 298 °K of the unit cell of dry MONADOR-2 are 0.52, 0.89 and 1.0 nm. The specific interlayer surface area and the interlayer CEC are 752 m²/g and 1.35 $mmol_C$/g respectively. The latter value is relatively close to the global CEC determined by hexaamminecobalt. The specific total surface area of this sample would be approximately the sum of the inner (XRD Theoretical surface) and outer (BET) area, and is equal to about 852 m² / g. The mean structural formula of this montmorillonite determined from chemical and mineralogical analyses is as follows:

$$\{Na_{0.57}K_{0.12}Mg_{0.10}Ca_{0.06}\}(Si_{7.79}Al_{0.21})\left[Al_{2.72}Fe^{III}_{0.29}Fe^{II}_{0.03}Ti_{0.02}\right]O_{20}\left|OH\right|_4 \quad (11)$$

{..}: Interlayer cations; (..): Tetrahedral layer; [..]: Octahedral layer.

The neutrality of the structural unit is ensured by the presence of compensation cations Na^+, Mg^{2+}, K^+ and Ca^{2+} in the interlayer space. It mainly contains sodium, but also shows non-negligible concentrations of potassium and magnesium.

The definition of the stability field of this montmorillonite is given by the electrophoretic mobility measurement as a function of pH (Fig. 7). Indeed, the dispersion and stability over time of a colloidal suspension are governed by a balance between van der Waals attractive forces and repulsive electrostatic forces. The monitoring of electrophoretic mobility indirectly reflects the evolution of this balance. In the pH range 6 to 9 used for water treatment, the montmorillonite MONADOR -2µm is

characterised by strong electrophoretic mobility and, consequently, its state of dispersion and stability is quite high. The electrophoretic mobility of this product remains negative throughout the pH range from 2 to 12. The main contribution to the overall surface charge of montmorillonite, and therefore to its mobility, is the permanent negative charge of basal surfaces due to isomorphic substitutions. This charge, which is not dependent either on the pH or on the ionic force, represents 90 to 95% of the overall charge. The different variations observed between pH 2 and 10 can be explained by the different contributions, according to the pH, of the charge of the lateral faces. The lateral surfaces have amphoteric silanol and aluminol sites. Their charge is dependent on the pH and the ionic force. These sites are therefore liable to participate in anion adsorption (low pH) or cation adsorption (higher pH). During observable variations, the diagram (pH, mobility) can be divided into three zones.

From 6 to 2, the decrease in electrophoretic mobility as the pH decreases is largely due to the saturation of the Si-O- bonds of the lateral faces with the formation of silanol groups, as well as to the ionisation of AlOH bonds ($AlOH \Leftrightarrow AlOH_2^+$).

From 6 to 9, the contribution of the charge of particle edges is very low and is almost nil at around 7.7 (pH determined by the second derivative). This pH, which is the maximum of the dome situated between 6 and 9, perfectly matches the PZC of the edges measured using the pH drift method (Table 1). This area is where the point of zero charge of the lateral faces forms.

Above pH 9, the increase in sodium concentration triggers the compression of the electrical double layer and subsequently a drop in electrokinetic potential and, thereby, in electrophoretic mobility. It is worth noting that the measurements taken below 3 and above 11 are greatly disturbed by the dissolution of the montmorillonite [40].

3.2 Statistical processing

The correlations between the different parameters determined in this study and the identification of the influence of each of them on adsorption were examined by principal component analysis (PCA). This

method provides a simple overview of objects considered according to all their known fields of variation. It can be used to sort the variables and reduce the number of parameters required to describe observations, minimising information loss. The correlations are summarised in Tables 2 and 3. The first process excluding CECs (Table 2) indicates that: (1) adsorption at pH 3 and 6.6 is strongly correlated, which can be expected as the interlayer charge remains negative and CIP is cationic at pH 3 and zwitterionic at pH 6.6 (Fig. 2. CIP in f(pH)); (2) the PZC has a moderate influence on CIP adsorption which leads to a low participation of the lateral faces in adsorption (ionisation of these faces in f(pH)); (3) the BET specific surface area has no influence as it represents the external surface area of the product in the case of observation with nitrogen; (4) the mesoporous volume has a very low effect; (5) the microporosity examined with nitrogen has an insignificant influence; (6) finally, the average dimension of pores or cracks has a negative influence on adsorption. Adsorption decreases as this dimension increases.

The same remarks apply to the second process including CECs and excluding activated carbon (Table 3); in addition the CEC plays a positive and very important role in CIP adsorption. The coefficient of determination between adsorption and CEC is 91%. The interlayer specific surface area of clay is therefore strongly and positively related to adsorption. The density of the interlayer charge is related to this parameter.

3.3 Adsorption isotherms

The adsorption isotherms are represented by the curve that gives the adsorption capacity at equilibrium Qe (mg/g) according to the concentration at equilibrium Ce (mg/L).

The adsorption isotherm obtained in Milli-Q water at pH 3 (Fig. 8) can be used to comparatively evaluate the adsorption capacity of smectite alone in an electrolyte-free medium where the smectite edges are mainly formed of positive aluminol sites and mainly neutral silanol sites.

Unlike the Langmuir model usually used in the literature, unsuited to heterogeneous surfaces such as those of clay, the D-A and Sips models adjust the experimental data extremely well with a coefficient of determination R^2 of 0.99. The maximum adsorption capacities obtained with the two models are practically identical. These two models represent the experimental results relatively well.

According to Gilles' classification of adsorption isotherms [41], the observed isotherm is classified as H2. The surface of the smectite MONADOR-2µm showed a strong adsorption affinity for ciprofloxacin. This adsorption was mainly marked by saturation of interlayer adsorption sites at low CIP concentrations.

As a first approximation, this isotherm can be described by three distinct regions: (1) an adsorption region with high relative energy represented by a vertical rise in the isotherm due to strong electrostatic interactions between the adsorbate and the adsorbent. These interactions take the form of the exchange of charge compensation cations with the ciprofloxacin. This CIP-CEC exchange was approximately 164 mg/g. The cation exchange capacity with CIP (CIP-CEC) was therefore 0.49 $mmol_C/g$; which constitutes almost one third of the CEC of MONADOR -2µm (1.386 $mmol_C/g$). The difference between these two CECs is related to CIP's molecular cross-sectional area as well as to its orientation between the sheets of this smectite. (2) An increasing adsorption region represented by a curved isotherm. The isotherm shape in this location characterises the presence of zones with heterogeneous surface energies, the most important rupture of which is located at a concentration, at equilibrium Ce, of between 8 and 20 mg/L. The majority of interactions in this area occur between the edges and the ciprofloxacin. Given the pH of the suspension, the reactional mechanisms are mainly van der Waals physical forces (dispersion forces) and hydrogen bonds [42,43]. (3) A constant adsorption region in which the isotherm reaches a plateau which, in this case, characterises the filling with a single layer of CIP.

The average maximum adsorption capacity was found to be approximately 374 ±30 mg/g, i.e. 1.13 ± 0.09 mmol/g. The surface energy heterogeneity index n_S, which was equal to 0.50 ±0.09, indicates that

the surface of this smectite is moderately heterogeneous. The adsorbate-adsorbent affinity constant K_S was 0.76 L/mg, which clearly shows that this smectite has a strong affinity for CIP. According to the D-A model, the overall adsorption energy was 25.4 ± 0.2 kJ/mol. This value is an average of the electrostatic energy (4 to 63 kJ/mol) [44], the hydrogen bond energy (4 to 13 kJ/mol) [45] and the van der Waals energy (2 to 4 kJ/mol) [45].

From three measurements taken in the Milli-Q water at pH 3, 6.5 and 10, the average maximum adsorption capacity can be estimated by the empirical equation Q max= 470.786 – 32.429*pH where $R^2 = 0.999$.

The tap water used for the following adsorptions had a pH of 8.1 ±0.1, a conductivity of 352 µS/cm at 25°C, an ionic force of 0.0054 ±0.0004 mol/L and a chemical composition with a dissolved salt concentration of 259 ±3 mg/L with 3.35 meq/L for cations and 3.51 meq/L for anions.

At pH 3 in the tap water, MONADOR -2µm had an H1 type isotherm with a low interlayer adsorption. Its saturation was relatively slow and its average maximum adsorption capacity was 318 ±15 mg/g, i.e. 0.98 ±0.09 mmol/g (Fig. 9). The affinity constant K_S in this environment was 0.41 L/mg, i.e. around half of its previous value. The surface energy heterogeneity index n_S was 0.41 ±0.02. Taking into account the uncertainties in the determination of this parameter in the Milli-Q water and the tap water at pH 3, the smectite was still moderately heterogeneous. According to the D-A model, the overall adsorption energy was 24 ±0.2 kJ/mol. The adsorption energy remains comparable to the previous value. The adsorption mechanisms still remained the same, however the adsorption capacity and adsorption rate of this pollutant were both slower and reduced by the presence of divalent cations, chlorides, sulphates and phosphates, which interacted with smectite at this pH.

At pH 3, the majority of cations were H^+, CIP^+, Ca^{2+} (41.3 mg/L), Mg^{2+} (5.7 mg/L), Na^+ (16.4 mg/L) and K^+ (4 mg/L). All these cations form a swarm around the smectite particles and can contribute to

the cation exchange process. However, given the concentrations of these cations, the exchange process in solution is continuous and increasingly slow as equilibrium is approached and is never fully achieved. All of these cations cause the flocculation of this product. The electrophoretic mobility in this state, measured by a Zetasizer NANO ZS, was found to be 0 µmcm/Vs with a conductivity of 1.02 ±0.01 mS/cm. According to the Schulze-Hardy Rule, the flocculating action of bivalent cations is far more energetic than that of monovalent cations. Given the diffusion rates of these cations, cation exchange occurs preferentially with the dissolved salt cations.

At pH 3 in tap water (Figs. 9 and 10), the MONADOR -2µm and MONADOR -20µm isotherms are practically identical and both are type H1 with very similar theoretical maximum adsorption capacities. This resemblance can be largely explained by the mineralogy of these two fractions. They contain respectively around 98% and 95% smectite.

At pH 3, CIP is positive, quartz is roughly neutral and albite has a very slightly negative electric charge. It is the permanent charge of smectite that prevails despite the presence of a slightly positive charge on the lateral faces. At this pH, the initial part of the isotherms of these two fractions is vertical. The quantity adsorbed appears to be high when the concentration of solute in the solution is close to zero. This phenomenon occurs when the interactions between the molecule adsorbed and the surface of the solid are very strong. This is in fact a cation exchange process. The Sips and D-A models adjust the experimental data perfectly, with a coefficient of determination R^2 of 0.999. In relation to Milli-Q water, adsorption became increasingly difficult due to the presence of dissolved salts and the decrease in available adsorption sites. For MONADOR -20 µm, the affinity constant K_S in this medium was 0.35 L/mg and the surface energy heterogeneity index n_S was 0.30 ±0.02. The decreases observed in relation to the previous values were also due to the presence of mineral impurities (5% Quartz and Albite). These mineral impurities increase the surface energy heterogeneity. According to the D-A model, the overall adsorption energy was 24 ±0.2 kJ/mol. This value remains comparable to the previous value. The adsorption mechanisms remain the same.

At pH 8, the isotherm of MONADOR -20µm in tap water is type S4, an interdependent adsorption isotherm (Fig. 10). At this pH, the two species $CIP^{\pm}$ and CIP^{-} were present in the water where the zwitterionic form of CIP was highly predominant. This pH also represents the point of zero charge of the lateral faces of MONADOR -2µm montmorillonite and that of the MONADOR -20µm matrix. According to Stillings [46], the PZC of albite is between 7 and 9. The shape of the isotherm does not indicate any cation exchange. This observation is corroborated by the fact that there is no shift in the peak (001) of the X-ray diffractograms obtained for the powder before and after CIP adsorption in tap water at pH 8 (Fig. 11). In both cases, d001 was 1.6 nm, which indicates an average of two-layer hydrate in the interlayer space [35]. In an alkaline environment, hydrogen may be replaced by another cation of the soluble salts present in tap water [47]. All of this information suggests that the CIP/salts/clay particle association is stabilised by hydrogen bonds and especially by complexation.

The isotherm has three points of inflection located at around 1.5, 12 and 22 mg/L (Fig. 10). The first part of this isotherm between 0 and 10 mg/L has a sigmoidal shape and can be modelled with Sips and D-A models. The second part can be modelled with a fifth order polynomial. The coefficient of determination ″R^2″ obtained with this polynomial was 0.9999.

For the first part, the affinity constant K_S was 0.43 ±0.03 L/mg, the index n_S was 1.74 ±0.08 and the adsorption energy was 22.8 ±0.2 kJ/mol. In this zone, CIP was in competition with the salts in the solvent to occupy the binding sites on the adsorbent. At low equilibrium concentrations (Ce<1.5 mg/L) the isotherm is convex. The direct adsorption of CIP is largely due to these salts. On the external basal surfaces of montmorillonite, CIP adsorption can occur in the hydration sphere of alkaline ions (adsorption in the form of outer sphere complexes [48]). On the lateral surfaces, the adsorption mechanism of the organic matter generally functions with pre-adsorbed ions in the form of inner sphere complexes. On the whole, outer sphere complexes employ electrostatic mechanisms (case of calcium) and are often less stable than inner sphere complexes, which use ionic bonding (case of

sodium). The average adsorption energy found by the D-A model can be attributed to a combination of adsorption energies which represent these two adsorption mechanisms. Furthermore, the isotherm shape (S) indicates the presence of lateral interactions. All of the CIP adsorption mechanisms result in cooperative interactions which are indicated indirectly by an n_S index greater than 1 and, in this case, of 1.74 ±0.08. This exponent can, in some cases, represent the formal number of molecules cooperating in such a "collaborative" interaction.

The second part of the isotherm, which is greater than 10 mg/L, shows two points of inflection. This shape characterises the presence of a multi-scale organisation of the CIP layers. The description of this assembly is based on the work of Singleton and Duval [49,50]. It consists in the two-dimensional condensation of CIP on the heterogeneous surface generated by the force of lateral adsorbate-adsorbate interactions.

The chemical composition of the tap water strongly contributes to the reduction in the adsorption of CIP by montmorillonite. The strong concentration of alkaline ions considerably reduces cation exchange between interlayer spaces and the outside. At alkaline pH, the screening of this area becomes a limiting factor on CIP adsorption.

4. Conclusion

In the experimental conditions of this study, the adsorption equilibrium between CIP and the sorbents studied depended on numerous factors, the main ones being the pH, the physico-chemical composition of the water, the overall specific surface area and the hydrodynamic conditions of the contact between the adsorbate and the adsorbent. Evidently, other factors affect adsorption such as surface chemistry, texture, pKa, electric charge density, electrokinetic potential, polarity, the concentrations used,

agitation duration, temperature, etc. For a given material, the adsorption mechanisms may vary according to the physico-chemical characteristics of the environment. The interactions between the adsorbate and the adsorbent may be either ionic (Coulomb forces) or non-ionic (van der Waals forces, hydrogen bonds, etc.).

Based on a correlation matrix established between 14 solids and 9 physico-chemical parameters, the principal component analysis clearly showed that when in contact with CIP, clay's CEC is a determining factor in the elimination of this molecule and the microporosity of the activated carbon is not involved in this process. There is no correlation between the adsorption capacities of the activated carbon and the volume of the micropores or the surface of the mesopores, which confirms the importance of the surface chemistry. The adsorption is therefore controlled by the volume of adsorbate as well as by its affinity for the adsorbent.

The comparison of adsorptions in open environments with strong agitation (600 s^{-1}), in Milli-Q water at pH 3 and 6.7, highlights the performances of MONADOR montmorillonite. This clay can be distinguished by its high crystallinity, a high CEC (1.4 mmolC/g) and a large specific surface area (800 m^2/g). Furthermore, it constitutes the main component of the sieved -20 µm fraction of MONADOR bentonite. It is natural, inert and readily available. It is therefore a key driver for the development of additional treatment processes balancing the retention of micropollutants similar to ciprofloxacin, the costs involved and environmental protection in its broadest sense. The -2 µm fraction, made of 98% sodium montmorillonite, could also be used in pharmaceutical and cosmetic sectors. In the same experimental conditions, sodium montmorillonite proved to be more efficient in terms of CIP adsorption than calcium montmorillonite. The affinity of Ca^{2+} for water is lower than than of Na^+, which is considered to have an unlimited hydration potential, liable to destabilise the sheet structure and facilitate exchanges. Adsorption in a closed environment (Batch) inevitably leads to adsorption rates which exceed the values obtained by experimentation in an open environment (Jar test).

In light of the energetic heterogeneity of the adsorbent surface, the location of adsorption sites and the range of CIP concentrations used, the Dubinin-Astakhov and Sips models were used to describe the macroscopic adsorption mechanisms. The Dubinin-Astakhov model does not assume that the surface is homogeneous or that the adsorption potential is constant as is the case for the Langmuir model. Its theory of volume filling of micropores is based on the fact that the adsorption potential is variable and the free enthalpy of adsorption is related to the degree of pore-filling. This isotherm assumes that the surface is heterogeneous. Based on the same principle as the Freundlich model, the Sips model is an empirical model which combines the Langmuir and Freundlich models in a single expression. The addition of an extra parameter in relation to the Langmuir and Freundlich models makes the Sips model more flexible and more efficient to describe experimental isotherms. In their field of application, the chosen models can be used to faithfully reproduce the experimental results of the equilibrium for CIP adsorption by MONADOR montmorillonite. The coefficient of determination between theory and experimental results (R^2) is 0.99.

Adsorption in tap water, the innovative element of this study, shows that MONADOR -20 µm bentonite shows a mean CIP adsorption rate of 184 ±6 mg/g, and can therefore compete with activated carbon. In economic terms, the extraction and mechanical preparation of this mineral fraction is far less costly than the use of activated carbon. The overall cost per tonne of this clay can be 6 to 30 times lower than that of activated carbon. The price bracket varies according to the quality of the activated carbon and transport costs. In terms of future prospects and prior to widespread application, the field of application would need to be extended to other pharmaceutical pollutants and semi-pilot industrial studies would have to be conducted.

Acknowledgments

This study was done within the framework of the POLPHARMA Project ANR-15-CE04-0007. The author gratefully acknowledges the French National Research Agency and the BRGM for financial support. He also wish to thank all those who contributed indirectly to the realization of this work.

REFERENCES

[1] T. Heberer, Occurrence, fate, and removal of pharmaceuticalresidues in the aquatic environment: a review of recent research data, Toxicology. Letters. 131 (2002) 5–17.

[2] A. Hartmann, A.C. Alder, T. Koller, R.M. Widmer, Identificationof fluoroquinolone antibiotics as the main source ofumuCgenotoxicity in native hospital wastewater, Environ. Toxicol. Chem. 17 (3) (1998) 377–382.

[3] T. aus der Beek, F.A. Weber, A. Bergmann, G. Grüttner, A. Carius, Pharmaceuticals in the environment: Global occurrence and potential cooperative action under the Strategic Approach to International Chemicals Management (SAICM), Umweltbundesamt. 2016. https://www.umweltbundesamt.de/en/publikationen/pharmaceuticals-in-the-environment-global

[4] SIPIBEL, Hospital effluents and urban wastewater treatment plants: characterization, risks and treatability, Report 2016.

http://www.graie.org/Sipibel/publications/sipibel-rapport-effluentshospitaliersmedicaments-oct16.pdf

[5] A.J. Watkinson, E.J. Murby, Costanzo, S. D. Removal of antibiotics in conventional and advanced waste water treatment: Implications for environmental discharge and wastewater recycling, Water Research. 41 (2007) 4164–4176.

[6] D.G.J. Larsson, Pollution from drug manufacturing: review and perspectives, Phil. Trans. R. Soc. B 369 (2014) 20130571.

[7] A. Khadra, E. Pinelli, M.Z. Lacroix, A. Bousquet-Melou, H. Hamdi, G. Merlina, M. Guiresse, M. Hafidi, Assessment of the genotoxicity of quinolone and fluoroquinolones Contaminated soil with the Vicia faba micronucleus test, Ecotoxicology and Environmental Safety. 76 (2012) 187–192.

[8] E. Kristiansson, J. Fick, A. Janzon, R. Grabic, C. Rutgersson, B. Weidegard, H. Söderström, D.G.J. Larsson, Pyrosequencing of antibiotic contaminated river sediments reveals high levels of resistance and genre transfer elements, PLoSONE 6 (2): e17038, 2011. https://doi.org/10.1371/journal.pone. 0017038

[9] C. Gu, K.G. Karthikeyan, Sorption of the antimicrobial ciprofloxacin to aluminum and iron hydrous oxides, Environ. Sci. Technol. 39 (2005) 9166–9173.

[10] S.A. Kumar, S.F. Wang, Adsorption of ciprofloxacin and its role for stabilizing multi-walled carbon nanotubes and characterization, Matter. Lett. 63 (2009) 1830–1833.

[11] C.J. Wang, Z. Li, W.T. Jiang, Adsorption of ciprofloxacin on 2:1 dioctahedral clay minerals, Applied Clay Science. 53 (2011) 723–728.

[12] Z. Li, H. Hong, L. Liao, C.J. Ackley, L.A. Schulz, R.A. MacDonald, A.L. Mihelich, S.M. Emard, A mechanistic study of ciprofloxacin removal by kaolinite, Colloids and surfaces B: Biointerfaces. 88 (2011) 339–344.

[13] C.L. Zhang, G.L. Qiao, F. Zhao, Y. Wang, Thermodynamic and kinetic parameters of ciprofloxacin adsorption onto modied coal fly ash from aqueous solution, Journal of molecular liquids. 163 (2011) 53–56.

[14] S.A.C. Carabineiro, T. Thavorn-amornsri, M.F.R. Pereira, J. L. Figueiredo, Comparison between activated carbon, carbon xerogel and carbon nanotubes for the adsorption of the antibiotic ciprofloxacin, Catalusis Today. 186 (2012) 29–34.

[15] S. Wu, X. Zhao, Y. Li, C. Zhao, Q. Du, J. Sun, Y. Wang, X. Peng, Y. Xia, Z. Wang, L. Xia, Adsorption of ciprofloxacin onto biocomposite fibers of grapheme oxide/calcium alginate, Chemical Engineering Journal. 230 (2013) 389–395.

[16] S. Rakshit, D. Sarkar, E. J. Elzinga, P. Punamiya, R. Datta, Mechanisms of ciprofloxacin removal by nano-size magnetite, J. Hazard. Mater. 246-247 (2013) 221– 226.

[17] W.T. Jiang, P.H. Chang, Y.S. Wang, Y. Tsai, J.S. Jean, Removal of ciprofloxacin from water by birnessite, J. of Hazard. Mater. 250-251 (2013) 362–369.

[18] STD.AFNOR X31-130-FREN 1999. Détermination de la capacité d'échange cationique (CEC) et des cations extractibles.

[19] A.L. Mular, R.B.A Roberts, simplified method to determine isoelectric points of oxides. Transactions of the Canadian Institute of Mining and Metallurgy, 69 (1966) 438–439.

[20] D. Balarak, F.K. Mostafapour, H. Azarpira, adsorption kinetics and equilibrium of ciprofloxacin from aqueous solutions using Corylusavellana (Hazelnut) activated carbon, British Journal of Pharmaceutical Research. 13 (3) (2016) 1–14.

[21] X. Yu, G.L. Zipp, G.W R. Davidson The effect of temperature and pH on the solubility of quinolone compounds: Estimation of Heat of Fusion. Pharma, Res. 11 (4) (1994) 522–527.

[22] R. Sips, On the Structure of a Catalyst Surface, J. Chem. Phys. 16 (1948) 490–495.

[23] M. Mahramanlioglu, I. Kizilcikli, I.O. Bicer, Adsorption of fluoride from aqueous solution by acid treated spent bleaching earth, Journal of Fluorine Chemistry. 115 (2002) 41–47.

[24] S. Mahapatra, K.N. Venugopala, T. N. Guru Row, A Device to Crystallize Organic Solids: Structure of Ciprofloxacin, Midazolam, and Ofloxacin as targets, Crystal Growth & Design. 10 (4) (2010) 1866–1870.

[25] L.R. Radovic, C. Moreno-Castilla, J. Rivera-Utrilla, Carbon materials as adsorbents in aqueous solutions. Chemistry and Physics of Carbon, Ed. L.R. Radovic, Marcel Dekker Inc, New York, 27 (2000) 227–405.

[26] S. Masson, C. Vaulot, L. Reinert, S. Guittonneau, R. Gadiou, L. Duclaux, Thermodynamic study of seven micropollutants adsorption onto an activated carbon cloth: Van't Hoff method, calorimetry, and COSMO-RS simulations, Environ. Sci. Pollut. Res. 24 (2017) 10005–10017.

[26] S. Wu, X. Zhao, Y. Li, C. Zhao, Q. Du, J. Sun, Y. Wang, X. Peng, Y. Xia, Z. Wang, Adsorption of ciprofloxacin onto biocomposite fibers of graphene oxide/calcium alginate, Chem. Eng. J. 230 (2013) 389–395.

[28] P. Ertl, B. Rohde, P. Selzer, Fast calculation of molecular polar surface area as a sum of fragment-based contributions and its application to the prediction of drug transport properties, J. Med. Chem. 43 (2000) 3714–3717.

[29] J.M. Cases, F. Villiéras, L. Michot, Les phénomènes d'adsorption, d'échange ou de rétention à l'interface solide–solution aqueuse, C. R. Acad. Sci. Paris, Sciences de la Terre et des planètes / Earth and Planetary Sciences. 331 (2000) 763–773.

[30] N. Kumar, M. P. Andersson, D. van den Ende, F. Mugele, I. Siretanu, Probing the surface charge on the basal planes of kaolinite particles with High-Resolution Atomic Force Microscopy, Langmuir 33 (2017) 14226−14237.

[31] R.F. Giese, Interlayer bonding in kaolinite, dickite and nacrite, Clays Clay Miner. 21 (1973) 145–149.

[32] M. Bizi, Stability and flocculation of nanosilica by conventional organic polymer, Natural Science. 4 (2012) 372–385.

[33] A.J. Carrasquillo, G.L. Bruland, A.A. Mackay, D. Vasudevan, Sorption of ciprofloxacin and oxytetracycline zwitterions to soils and soil minerals: Influence of compound structure, Environ. Sci. Technol. 42 (2008) 7634–7642.

[34] T. Watanabe, T. Sato, Expansion characteristics of montmorillonite and saponite under various relative humidity conditions, Clay Science. 7 (1988)129–138.

[35] D.W. Ruthrford, C.T. Chiouet, D.D. Eberl, Effects of exchanged cation on the microporosity of montmorillonite, Clays and Clay Minerals. 45 (4) (1997) 534–543.

[36] S.L. Swartzen-Allen, E. Matijevic, Surface and colloid chemistry of clays, Chemical Reviews, 74 (3) (1974) 385–400.

[37] D.W. Smith, Ionic hydration enthalpies, J. Chem. Educ. 54 (9) (1977) 540–542.

[38] W. Müller, J. Flesch, W. Meyer, Treatment of intershell correlation effects in ab initio calculations by use of core polarization potentials. Method and application to alkali and alkaline earth atoms, J. Chem. Phys. 80 (1984) 3297–3310.

[39] X. Zhang, H. Yi, Y. Zhao, F. Min, S. Song, Study on the differences of Na- and Ca-montmorillonites in crystalline swelling regime through molecular dynamics simulation, Advanced Powder Technology 27 (2016) 779–785

[40] M.L. Rozalen, F.J. Huertas, P.V. Brady, J. Cama, S. Garcia-Palma, J. Linares, Experimental study of the effect of pH on the kinetics of montmorillonite dissolution at 25 °C, Geochim. Cosmochim. Acta. 72 (2008) 4224–4253.

[41] C.H. Giles, D. Smith, A. Huitson, A General Treatment and Classification of the Solute Adsorption Isotherm. I. Theoretical, J. Colloid Interface Sci. 47 (3) (1974) 755–765.

[42] T. Steiner, The Hydrogen Bond in the Solid State, Angew. Chem. Int. Ed. 41 (2002) 48–76.

[43] J.J. Holstein, C.B. Hübschle, B. Dittrich, Electrostatic properties of nine fluoroquinolone antibiotics derived directlyfrom their crystal structure refinements, CrystEngComm 14 (2012) 2520–2531.

[44] G.H. Desiraju, Hydrogen Bridges in Crystal Engineering: Interactions without borders, Acc. Chem. Res. 35 (2002) 565–573.

[45] J.M. Berg, J.L. Tymoczko, L. Stryer, Biochemistry 5th edition, W. H. Freeman, New York, 2002, Section 1.3, Chemical Bonds in Biochemistry, pp. 43–44.

[46] L.L. Stillings, S.L. Brantley, M.L. Machesky, Proton adsorption at an adularia feldspar surface. Geochim, Cosmochim. Acta. 59 (1995) 1473–1482.

[47] S. Caillère, S. Henin, M. Rautureau, Minéralogie des argiles, Tome I. Edition Masson, 1982, p. 161.

[48] F. Coppin, S. Castet, G. Berger, M. Loubet, Microscopic reversibility of Sm and Ybsorption onto smectite and kaolinite: an experimental evidence, Geochim. Cosmochim. Acta. 67 (2004) 2515–2527.

[49] I.H. Singleton, G.D. Halsey, The solution of argon in layers of Krypton, J. Phys. Chem. 58 (11) (1954) 1011–1017.

[50] X. Duval, A. Thomy, The Interpretation of Krypton Adsorption Isotherms on Exfoliated Graphite, Carbon 13 (1975) 242–243.

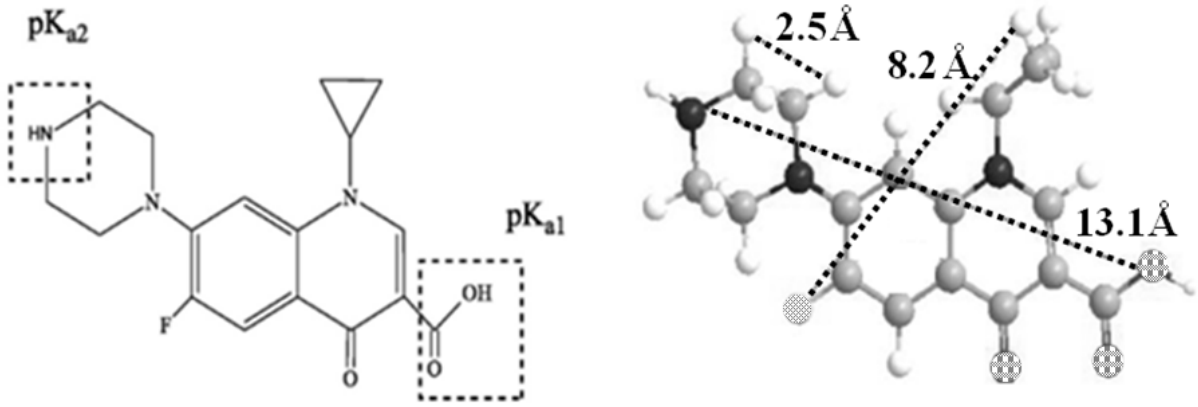

Fig. 1. Chemical molecular formulae and structure of CIP (The molecular dimension size of L13.1 Å x W8.2 Å x H2.5 Å) [67].

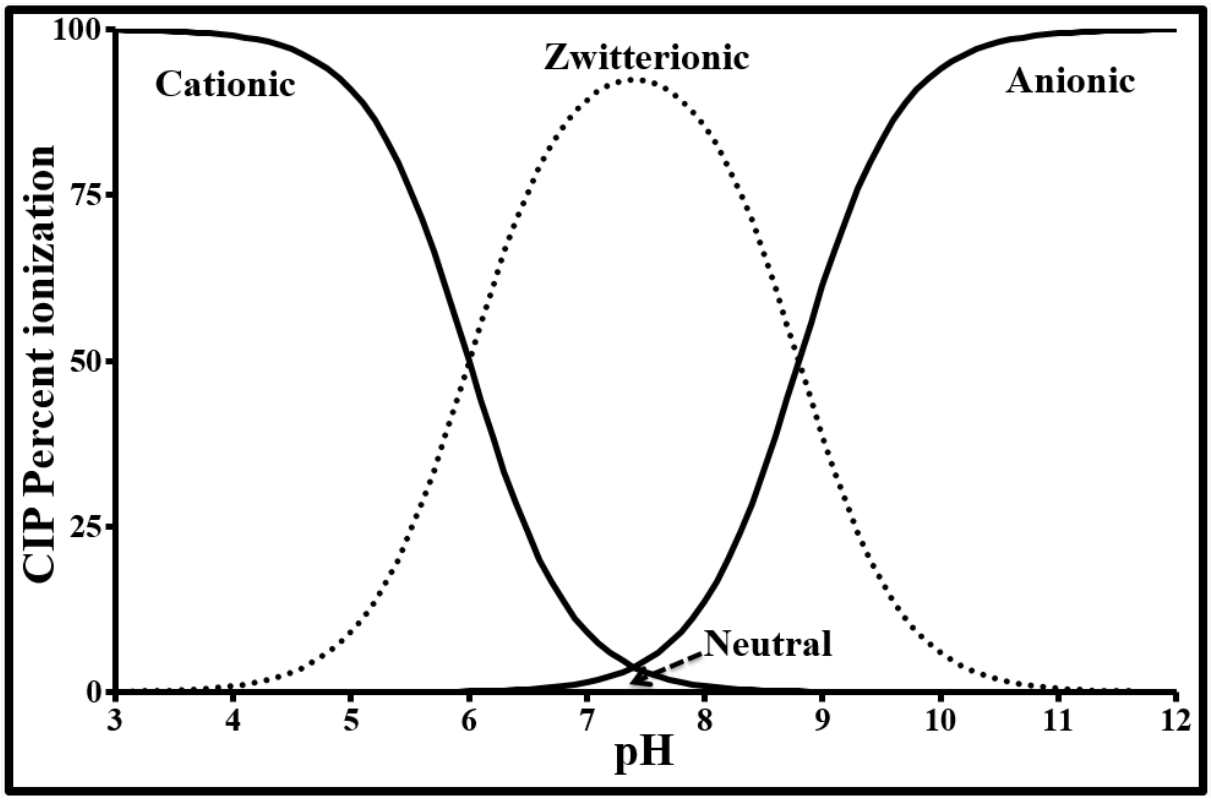

Fig. 2. Ciprofloxacin speciation under different pHs in aqueous solution.

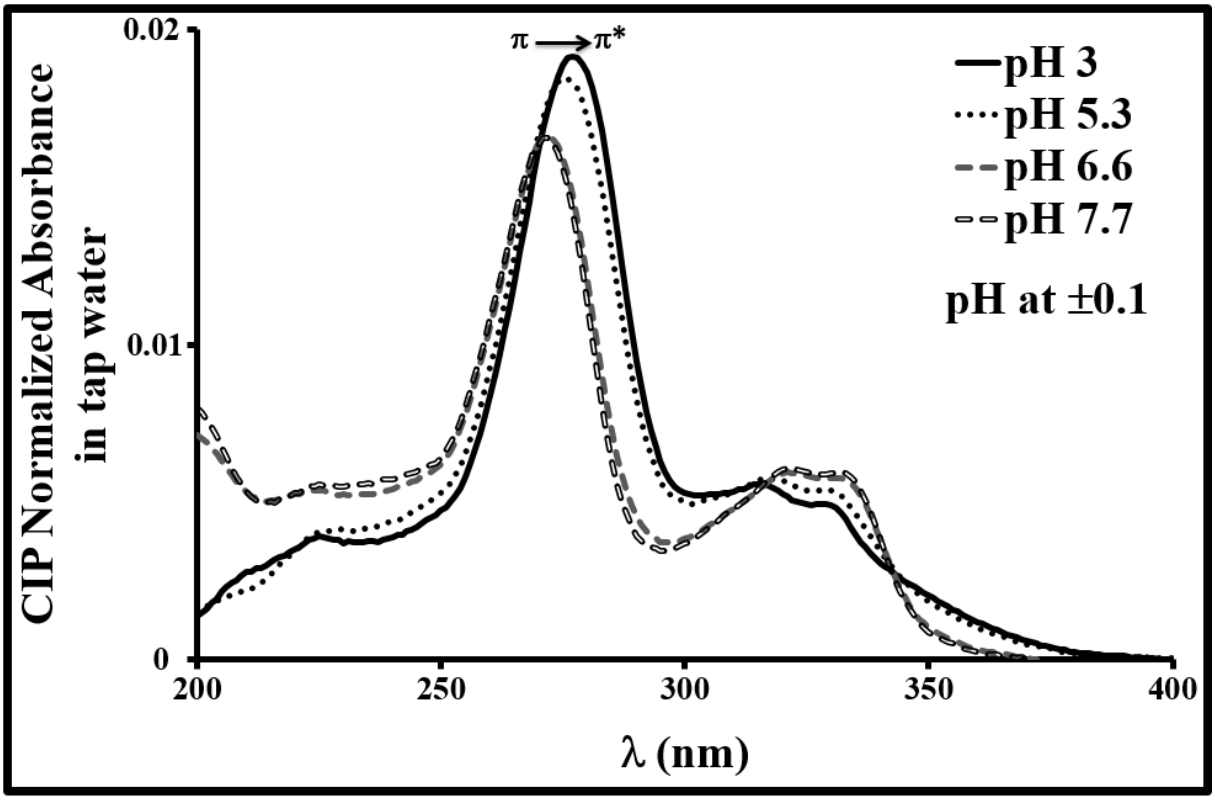

Fig. 3. Ciprofloxacin absorption spectra in tap water as a function of 4 pHs.

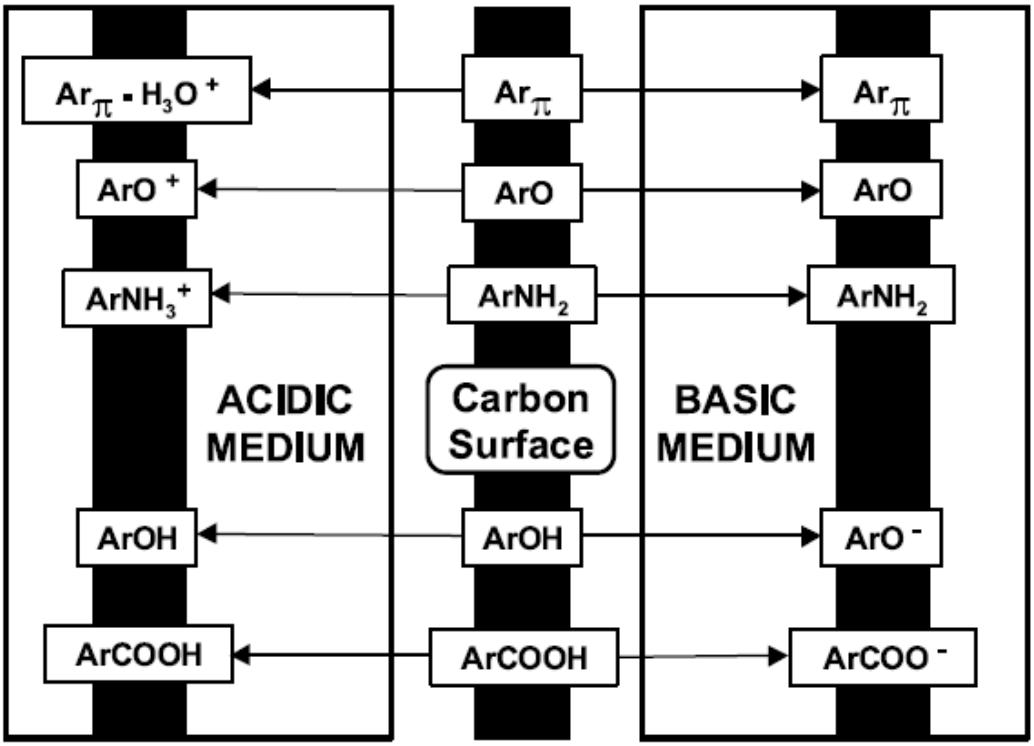

Fig. 4. Macroscopic representation of the features of carbon surface chemistry [82].

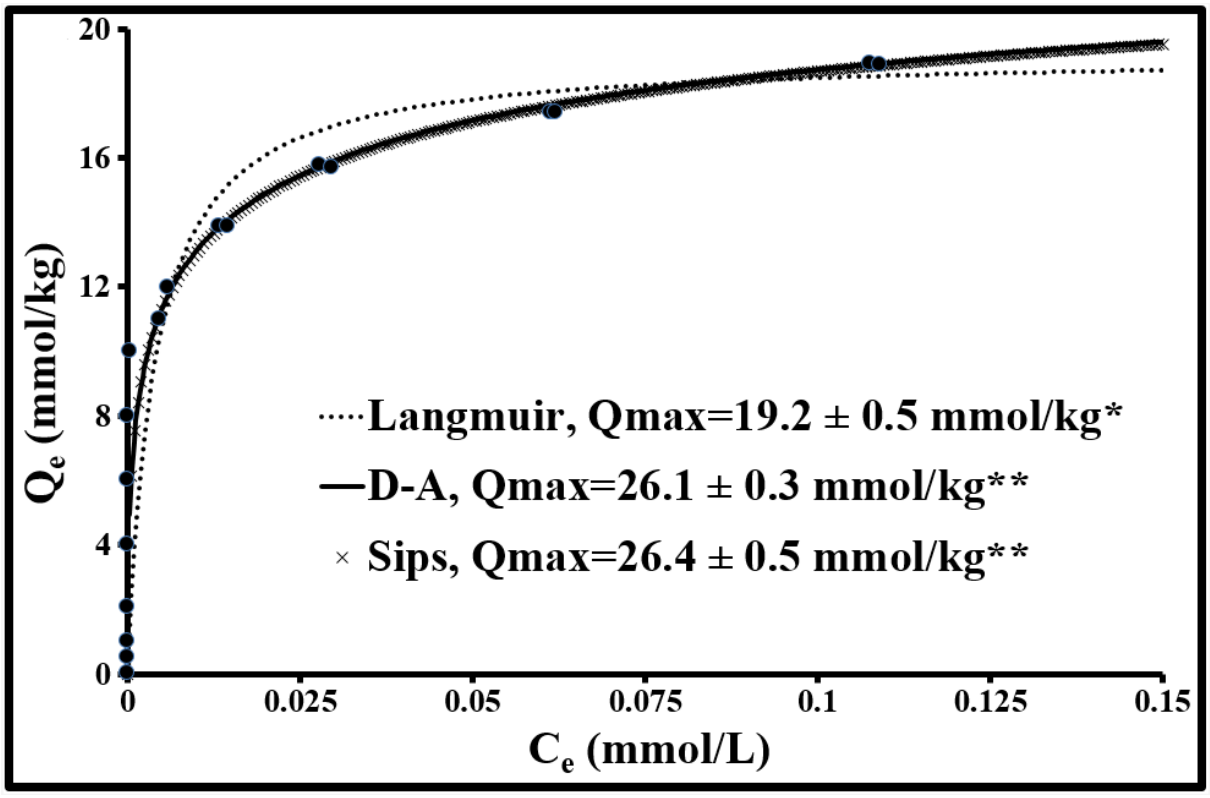

Fig. 5. CIP adsorption isotherm on kaolinite KGa-2 at pH 3.5 in aqueous solution with MilliQ water. * Li et al., 2011; ** This work.

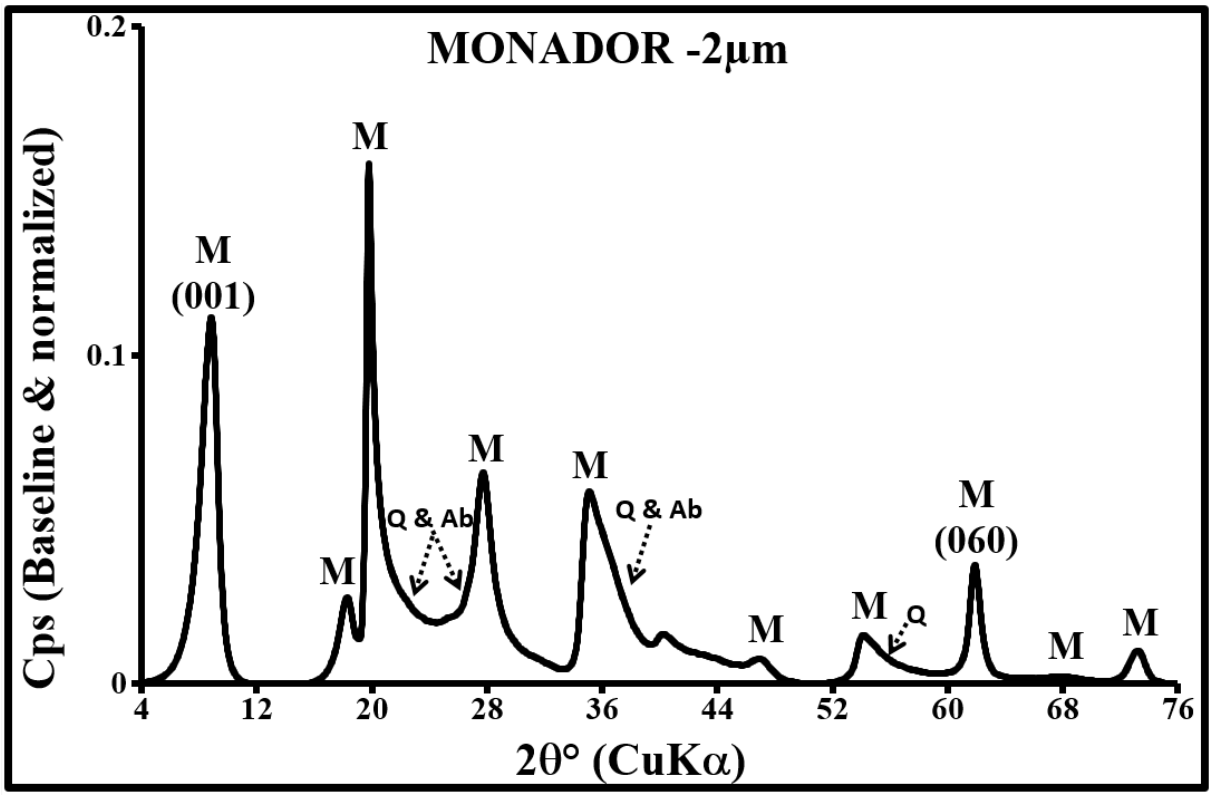

Fig. 6. XRD diffraction patterns of montmorillonite MANADOR (F= Feldspar; M= montmorillonite; Q= Quartz).

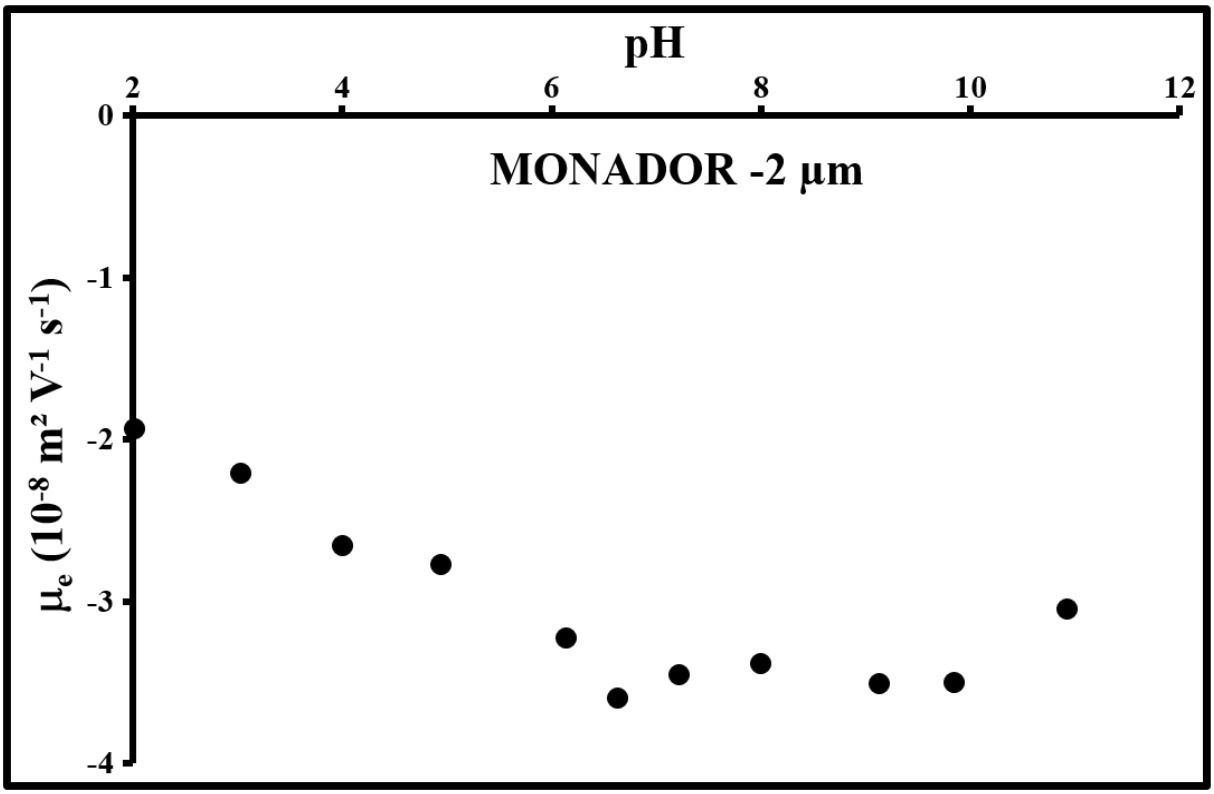

Fig. 7. Electrophoretic mobility of montmorillonite MANADOR in Milli-Q water solution.

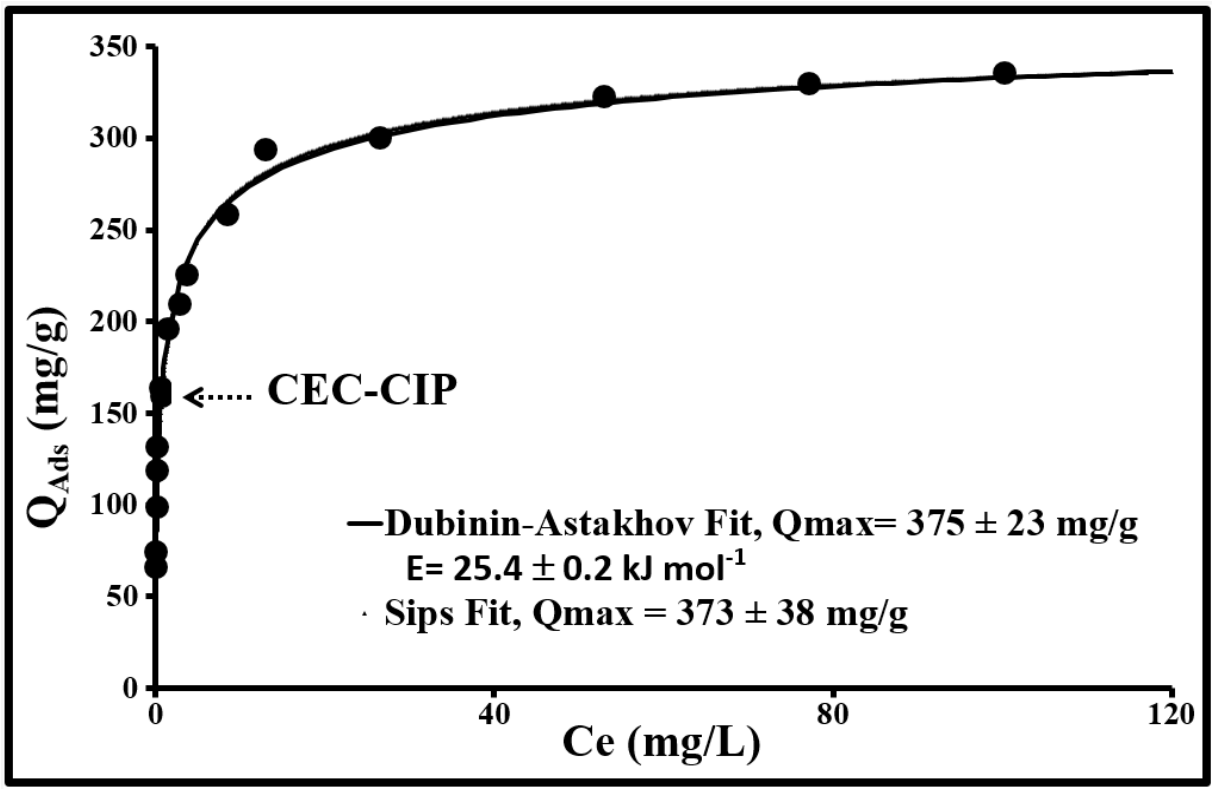

Fig. 8. CIP adsorption isotherm on MONADOR-2µm at pH 3 in Milli-Q water solution.

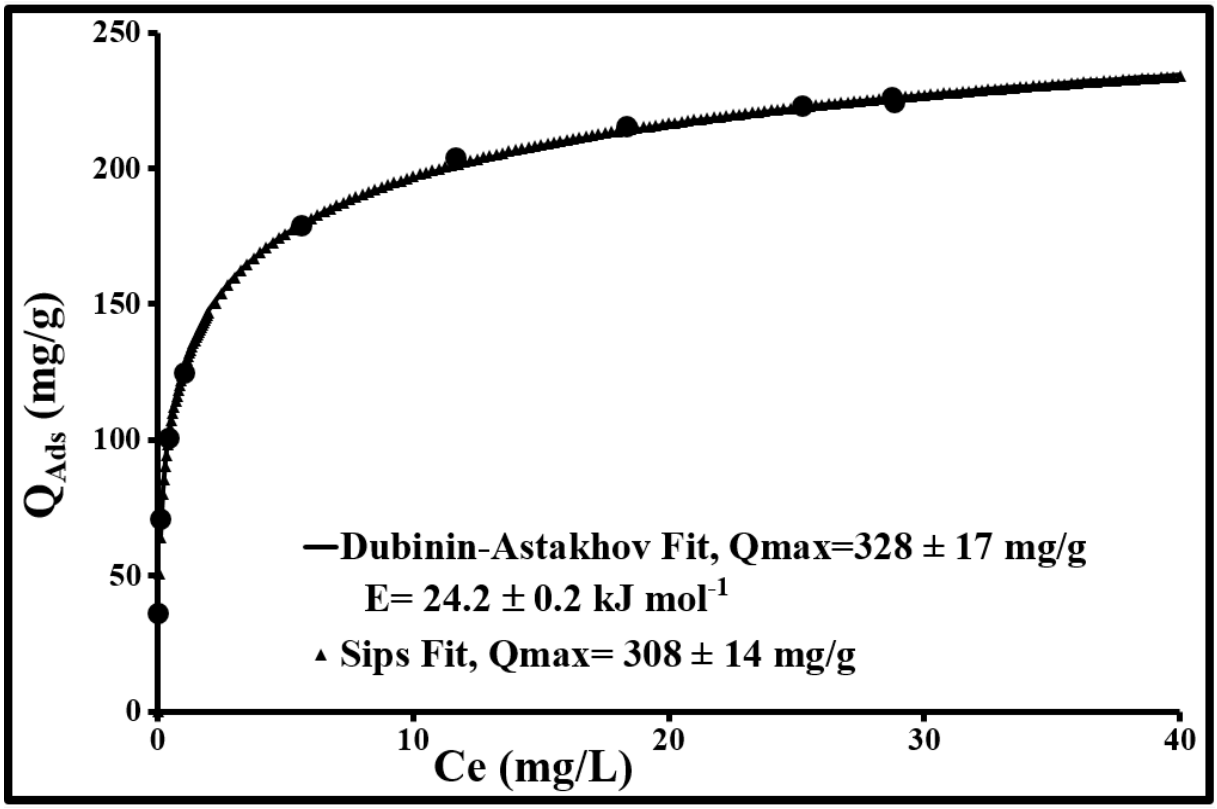

Fig. 9. CIP adsorption isotherm on MONADOR-2µm at pH 3 in in tap water solution.

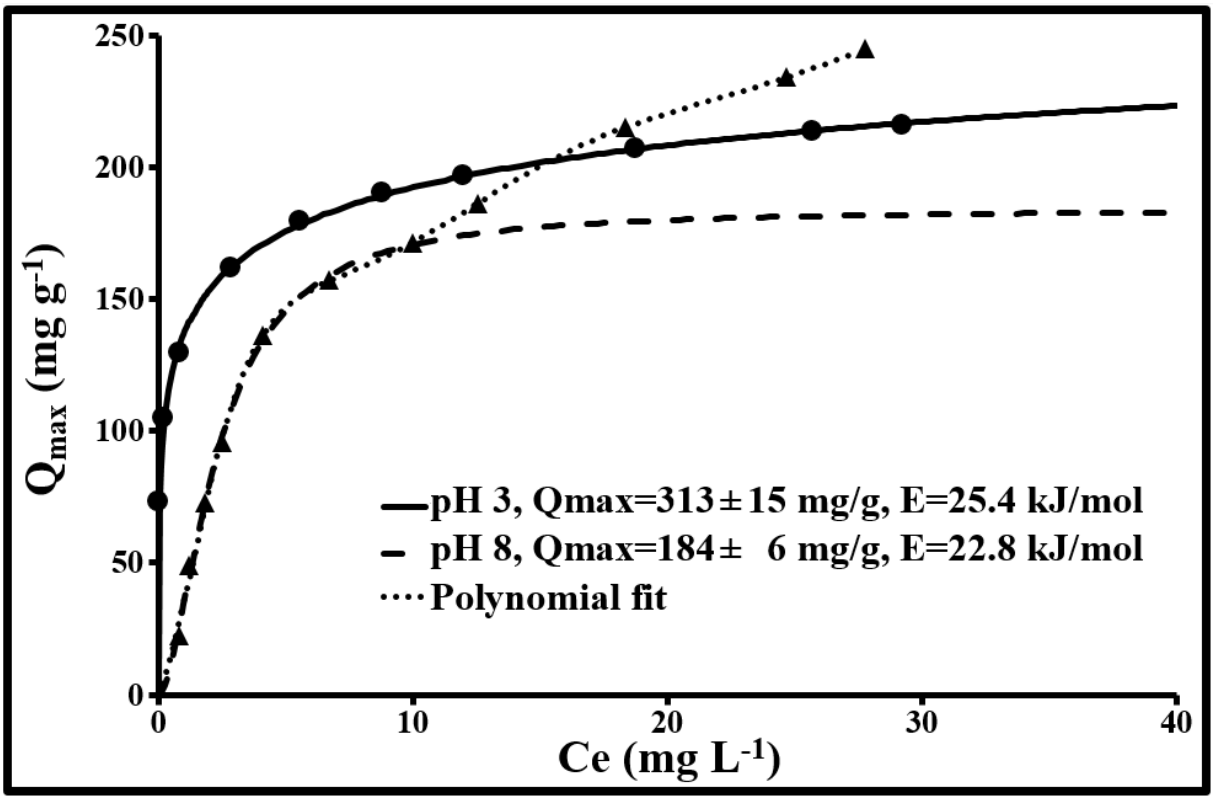

Fig. 10. CIP adsorption isotherm on MONADOR-20µm at pH 3 and 8 in tap water solution.

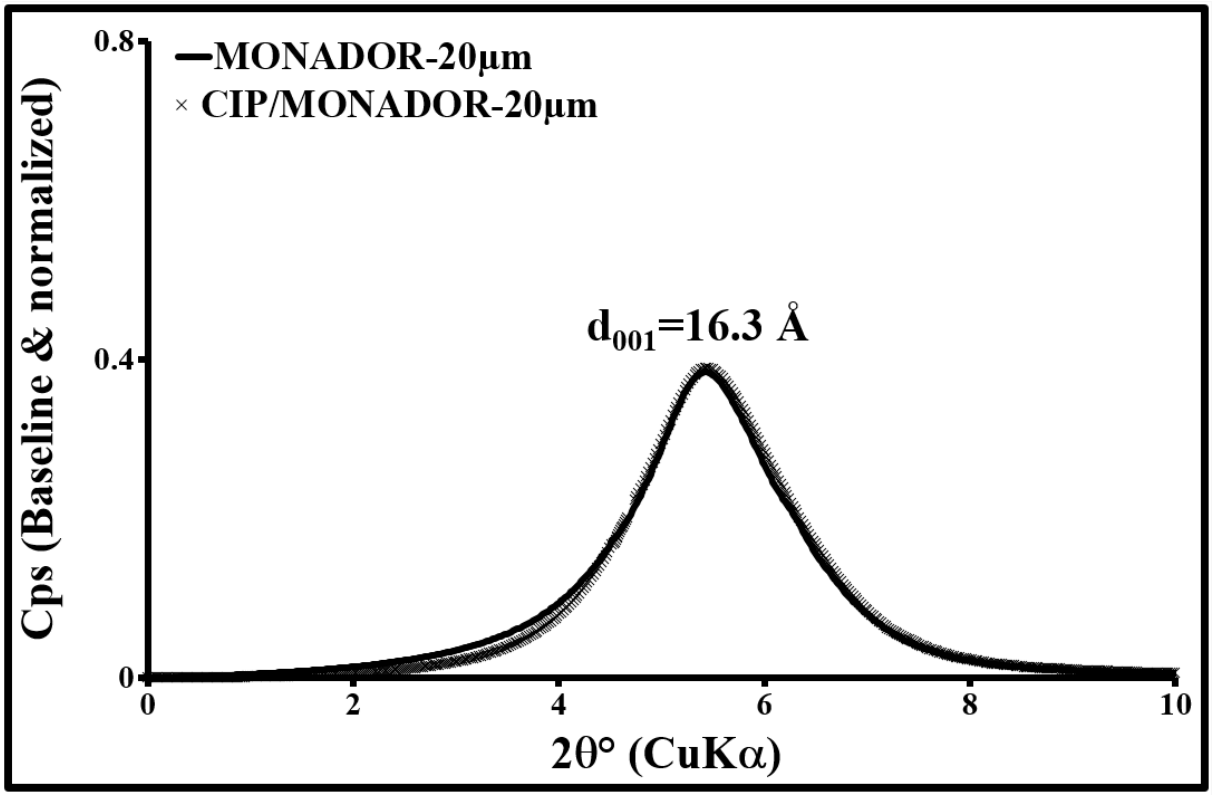

Fig. 11. XRD diffraction patterns showing the 001 reflection of MONADOR-20µm before and after CIP adsorption in tap water solution.

Table 1

Limit adsorptions obtained in Jar-test at 600 S^{-1}, pH 3, pH 6.5 and textures of the selected products.

Adsorbent	Q3	Q6.5	PZC	CEC	SS_{BET}	C	$SS_{\mu P}$	$L_{\mu\text{-t-plot}}$	V_{PT}	$V_{\mu P}$	V_{mP}
	mg/g	mg/g		$mmol_C/g$	m^2/g		m^2/g	nm	cm^3/g	cm^3/g	cm^3/g
CAP1	216	207	8.4	n.c	979.0	1062	884.6	1.69	0.46	0.37	0.09
CAP1-20	197	218	8.2	n.c	941.5	849	831.4	1.70	0.46	0.35	0.10
CAP2	257	256	6.8	n.c	957.2	989	694.6	1.75	0.58	0.30	0.28
CAP2-20	243	269	6.9	n.c	987.3	721	693.5	1.74	0.62	0.30	0.32
Diatomite	45	46	6.1	n.c	9.8	462	0.0	0.00	0.02	0.00	0.02
K7A	48	44	4.0	0.043	14.5	305	5.5	0.93	0.07	0.00	0.07
MONADOR-20	230	248	8.0	1.412	87.7	479	42.1	0.87	0.11	0.02	0.09
MONADOR-2	238	263	7.9	1.386	99.2	499	56.5	0.86	0.11	0.02	0.09
Na-MONADOR-2	253	283	7.2	1.325	110.2	557	67.6	0.88	0.10	0.03	0.07
Ca-MONADOR-2	188	208	6.9	1.368	90.0	471	54.6	0.87	0.09	0.02	0.07
Rassoul-20	158	170	8.3	0.644	188.2	355	107.0	0.90	0.10	0.05	0.05
Na-Rassoul-2	169	194	9.2	0.804	202.0	519	98.5	0.96	0.15	0.05	0.10
SWy3-20	193	214	7.0	0.785	41.9	461	12.5	0.98	0.09	0.01	0.08
SWy3-2	204	224	7.4	0.998	43.8	380	12.0	1.01	0.09	0.01	0.08

Q: adsorption limite (pH 3 and 6.5). PZC: Point of zero charge. CEC: Cation exchange capacity. SS_{BET}: BET Specific surface area. C: BET Energy constant. $SS_{\mu P}$: Equivalent specific surface area of micropores obtained by application of t-plot method. $L_{\mu\text{-t-plot}}$: Mean equivalent pore width (t-Plot). V_{PT}: Total specific pore volume at P/P0= 0.97. $V_{\mu P}$: Specific micropore volume (t-Plot). V_{mP}: Specific mesopore volume (BJH). n.c: not concerned.

Table 2

Correlation matrix without CEC for coefficient estimates (All adsorbent).

Adsorbent	Q3	Q6.6	PZC	SS_{BET}	C	$SS_{\mu P}$	$L_{\mu\text{-t-plot}}$	V_{PT}	$V_{\mu P}$	V_{mP}
Q3	1									
Q6.6	**0.989**	1								
PZC	**0.550**	**0.568**	1							
SS_{BET}	0.435	0.356	0.246	1						
C	0.494	0.397	0.306	**0.911**	1					
$SS_{\mu P}$	0.396	0.312	0.253	**0.989**	**0.926**	1				
$L_{\mu\text{-t-plot}}$	**0.597**	0.532	0.244	**0.880**	**0.765**	**0.863**	1			
V_{PT}	0.490	0.417	0.176	**0.979**	**0.868**	**0.944**	**0.896**	1		
$V_{\mu P}$	0.400	0.317	0.253	**0.992**	**0.926**	**1.000**	**0.867**	**0.949**	1	
V_{mP}	0.523	0.488	-0.005	**0.704**	**0.540**	**0.601**	**0.716**	**0.831**	**0.614**	1

In bold, significant values (except diagonal) at the level of significance alpha=0.050 (Two-tailed test)

Table 3

Correlation matrix for coefficient estimates (Only for clay).

Adsorbent	**Q3**	**Q6.5**	**PZC**	**CEC**	**SS_{BET}**	**C**	**$SS_{\mu P}$**	**$L_{\mu\text{-t-plot}}$**	**V_{PT}**	**$V_{\mu P}$**	**V_{mP}**
Q3	1										
Q6.6	**0.998**	1									
PZC	0.634	0.652	1								
CEC	**0.918**	**0.911**	0.530	1							
SS_{BET}	0.203	0.230	**0.779**	0.158	1						
C	**0.778**	**0.803**	0.552	**0.756**	0.352	1					
$SS_{\mu P}$	0.220	0.243	**0.701**	0.206	**0.978**	0.358	1				
$L_{\mu\text{-t-plot}}$	-0.309	-0.288	-0.078	-0.509	-0.259	-0.353	-0.417	1			
V_{PT}	0.385	0.419	**0.828**	0.357	**0.754**	0.639	0.652	-0.068	1		
$V_{\mu P}$	0.196	0.222	**0.713**	0.173	**0.989**	0.353	**0.998**	-0.361	**0.682**	1	
V_{mP}	0.316	0.335	0.374	0.303	-0.016	0.495	-0.163	0.288	0.640	-0.126	1

In bold, significant values (except diagonal) at the level of significance alpha=0.050 (Two-tailed test)

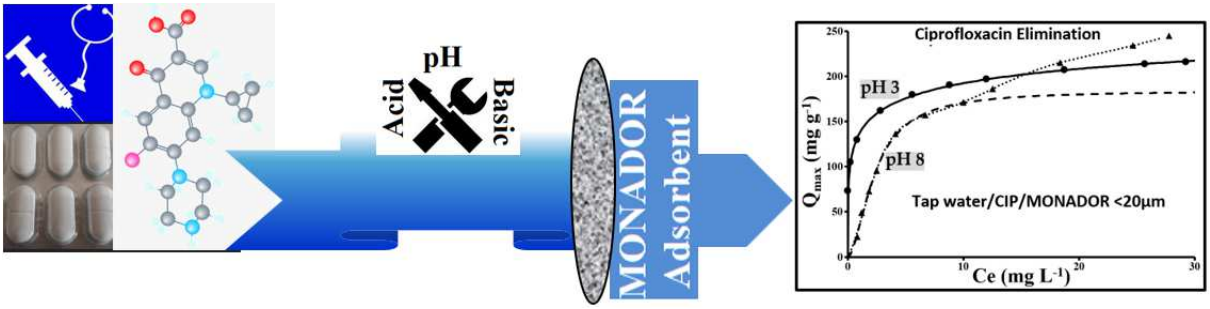
pH
Acid
Basic
MONADOR
Adsorbent
Ciprofloxacin Elimination
pH 3
pH 8
Tap water/CIP/MONADOR <20µm
Q_{max} (mg g^{-1})
Ce (mg L^{-1})
0
50
100
150
200
250
10
20
30